Kanamaru *et al. Earth, Planets and Space* (2022) 74:53
https://doi.org/10.1186/s40623-022-01618-1

Earth, Planets and Space

EXPRESS LETTER

Open Access

# Magnetic petrology of pumice fall deposits of the 1783 eruption of Asama volcano, Japan

Tatsuo Kanamaru[1*], Kuniyuki Furukawa[2], Xiangyu Zhao[3,4] and Yusuke Suganuma[3,5]

**Abstract**

Magnetic petrological investigations were conducted on the pumice fall deposits of the 1783 eruption of Asama volcano to examine relationships between bulk magnetic properties and petrological features related to the magmatic and volcanic processes of the eruption. The magnetic properties of the deposits agree with the mineralogical investigation, indicating the existence of titanomagnetite and pyrrhotite as magnetic minerals in the deposits. Although most magnetic properties are common over depositional units, mass-specific magnetic susceptibility decreases as the eruption progressed, implying a change in titanomagnetite abundance. This is consistent with a previously proposed binary magma mixing model and is because of the increasing mafic endmember component without titanomagnetite. Our results demonstrate that magnetic petrology can be a useful tool for investigating volcanic and magmatic processes.

**Keywords:** Asama volcano, 1783 eruption of Asama volcano, Pumice, Opaque mineral, Fe–Ti oxide, Titanomagnetite, Pyrrhotite, Magnetic petrology, Magnetic property

**Graphical Abstract**

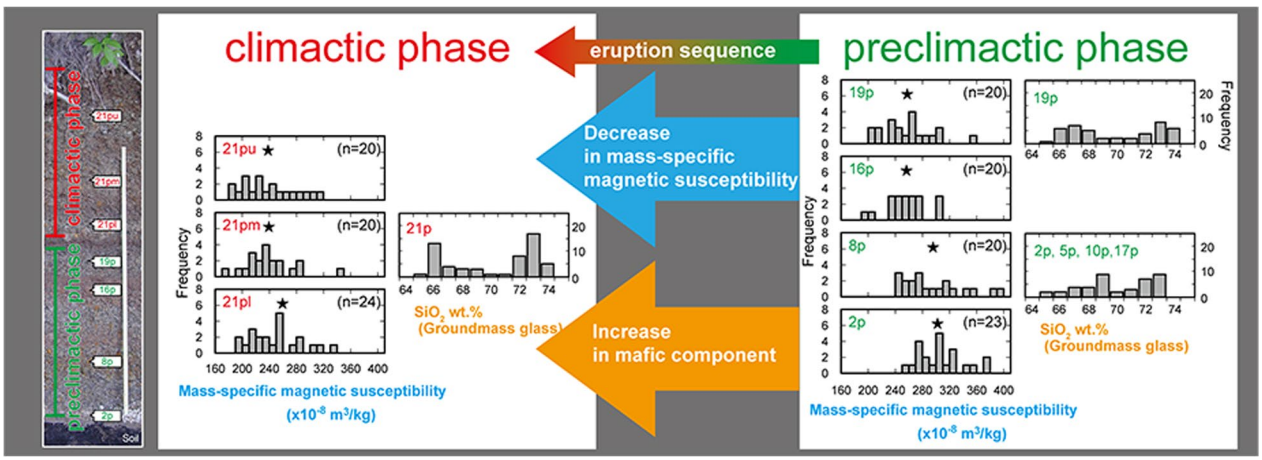


## Introduction

The existence of opaque minerals in pyroclastic deposits can be used to investigate the magmatic evolution and emplacement mode of pyroclastic deposits. For example, Nakamura (1995) estimated the time scale of magma

*Correspondence: kanamaru.tatsuo@nihon-u.ac.jp
[1] Department of Earth and Environmental Sciences, College of Humanities and Sciences, Nihon University, 3-25-40, Sakurajosui, Setagaya-ku, Tokyo 156-8550, Japan
Full list of author information is available at the end of the article

mixing at the Unzen volcano using the diffusivity of the ulvöspinel component of titanomagnetite (TM), which showed chemical zoning. Turner et al. (2008) also discussed the relationship between eruptive style and exsolution texture of TM in pyroclastic deposits. Magnetic properties of these deposits, such as magnetic susceptibility, magnetic coercivity, Curie/Néel temperature, magnetic hysteresis properties, and so on, are proxies for chemical composition, abundance, grain size, and texture of magnetic minerals (e.g., Nagata 2013). The study of petrology and mineralogy of rocks, such as magnetic minerals, and their magnetic properties is called magnetic petrology (Frost 1991). Thus, magnetic petrological studies of pyroclastic deposits can elucidate their mode of emplacement (e.g., Saito et al. 2007).

Asama volcano is located approximately 100 km from Tokyo, Japan (Fig. 1a). The volcano's most recent large eruption occurred in 1783. Fortunately, the eruptive sequence of the eruption, which caused disasters at the foot of the mountain and the metropolitan area, was well depicted in old documents, which were consistent with well-preserved geological strata. Several persistent investigations from various viewpoints are expected to understand volcanic processes to reduce volcanic hazards because erupting volcanoes can cause disaster in metropolitan areas. Thus, in this study, we conducted the first magnetic petrological investigation for Asama volcano to reveal the relationship between magmatic petrological features and magmatic processes. Additionally, we show that magnetic petrological studies can be a useful tool for detecting the transition of magmatic and/or eruptive conditions in an expected future eruption. We chose pumice fall deposits from the eruption for this study because the deposits' opaque minerals, which act as magnetic carriers, are expected to retain the original character of its magmatic conditions because of quenching immediately after the eruption.

## 1783 eruption of Asama volcano

Asama volcano (Fig. 1a) is composed of three volcanic edifices, Kurofu (ca. 100–20 ka), Hotokeiwa (ca. 20–10 ka), and Maekake (in chronological order) (Aramaki 1963). Maekake volcano is an andesitic stratovolcano active from ca. 10 ka to now (Yasui and Koyaguchi 2004; Takahashi et al. 2008, 2013). The 1783 eruption of the Asama volcano, which erupted from the Maekake volcano, is the youngest largescale eruption of the Asama volcano (Yasui and Koyaguchi 2004). Based on analyses of old documents and geological surveys, the following is an estimated outline of the eruptive sequence: (e.g., Aramaki 1956, 1957; Imai and Mikada 1982; Tamura and Hayakawa 1995; Yasui and Koyaguchi 2004; Tsukui 2010). The eruption began on May 9 (or possibly 8) in 1783 and lasted for approximately 3 months, until the morning of August 5. Before nighttime of August 4, minor- to mid-scale eruptions continued intermittently. During this period, pyroclastic (ash and pumice) fell in the NE, NNW, and ESE directions. Minor pyroclastic flows were also generated in this period. A climactic eruption occurred from the nighttime of August 4 to the next morning. During the climactic eruption, the main portion of Agatsuma pyroclastic flow, Onioshidashi lava, and the main portion of the ESE pyroclastic fall deposit was emplaced. A pyroclastic and debris avalanche flow (Kambara flow) devastated a village in the northern foothills of Asama volcano immediately after the climactic eruption (Fig. 1a). In terms of the magma process, the whole-rock chemical composition of the eruptive products changed from relatively felsic to mafic at the end of the eruption. The change in magmatic chemical composition was mainly due to binary magmatic mixing during the eruption (Aramaki and Takahashi 1992; Yasui and Koyaguchi 2004).

## Methods

### Materials

Yasui et al. (1997) and Yasui and Koyaguchi (2004) identified 22 units (14 pumice fall units and eight ash fall units) for the ESE pyroclastic fall deposit. Based on their classification, we sampled pumice fall deposits from five pumice fall units (2p, 8p, 16p, 19p, and 21p) from an outcrop adjacent to the Asama volcano observatory (AVO) of the University of Tokyo (Fig. 1a, b). Furthermore, we divided the unit 21p into three subunits from the bottom to top, which are lower (21pl), middle (21 pm), and upper (21pu), respectively. Therefore, we sampled the pumice fall deposits from seven units on the outcrop. According to Yasui and Koyaguchi (2004), the 21p (21pl, 21pm, and 21pu in this study) is ejecta from the climactic eruption. Therefore, the 2p, 8p, 16p, and 19p are preclimactic eruption products. To eliminate pumice oxidized after the eruption, small pieces of pumice with a long axis of 1–1.5 cm were selected for our experiments (Fig. 1c). This is because the inner part of the large pumice is often pinkish, owing to oxidation.

### Magnetic property measurements

To clarify the magnetic properties of the pumice fall deposits, several types of rock magnetic experiments, microscopic observations, and mineralogical analyses were conducted on selected samples. Mass-specific magnetic susceptibility (MS) was measured with a magnetic susceptibility measurement system (MS2B; Bartington) at Nihon University. For the MS measurement, 20–24 pieces of pumice were measured for each unit (Fig. 1d). At the National Institute of Polar Research (NIPR),

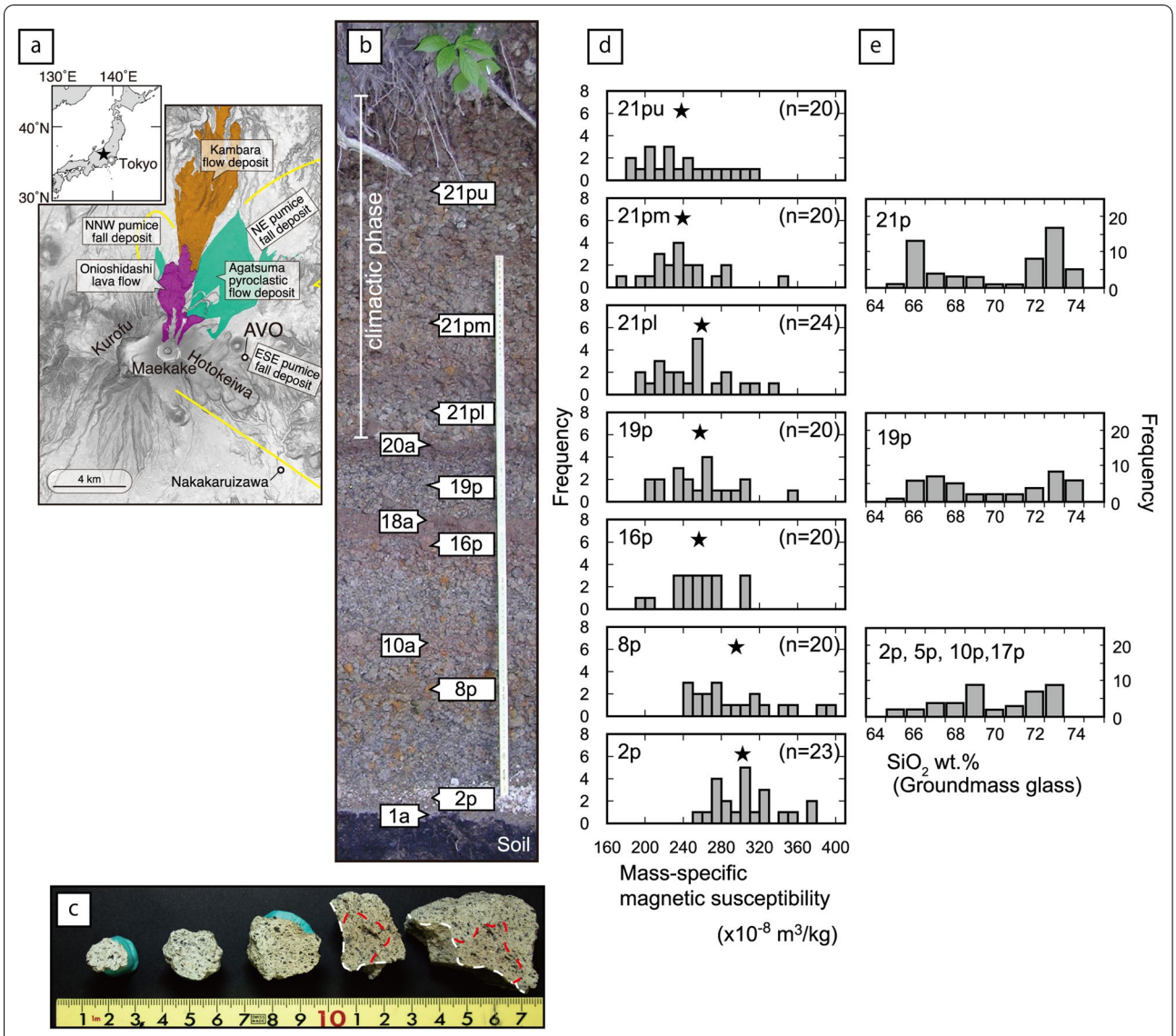


**Fig. 1** **a** Topographic map of Asama volcano consisting of Kurofu volcano, Maekake volcano, and Hotokeiwa volcano. The star in the index map upper left shows the location of the Asama volcano. The distribution of the 1783 eruptive products (Aramaki 1993) is shown. Yellow lines indicate 1 cm isopach of the pumice fall deposits from the 1783 eruption (Yasui and Koyaguchi 2004). *AVO* Asama volcano observatory. **b** Photograph showing the occurrence of the ESE pumice fall deposits of the eruption. Letters shown on the photograph indicate the sampled units for this study. The distinctive ash fall deposits shown in Yasui and Koyaguchi (2004) are also shown. The scale bar on the right is 1 m long. **c** Representative halved sections of pumice samples of various sizes. Pumice samples with the same size as or smaller than the smallest one in this figure were used for this study. White dashed lines indicate broken-out sections of the large samples. Pinkish oxidized parts are surrounded by red dashed line. **d** Histograms showing the frequency of magnitude of MS of pumice fall deposits. The stars in the diagrams represent the average values. **e** Histograms showing $SiO_2$ content of groundmass glass composition of each unit. This is rewritten from Fig. 3 in Yasui (2016) with permission from the Institute of Natural Sciences, College of Humanities and Sciences, Nihon University

isothermal remanent magnetization (IRM) acquisition curves and hysteresis loops were measured with a maximum magnetization field of 1 T using an alternating gradient magnetometer (AGM) (MicroMag 2900, Princeton Measurement Corp). IRM acquisition curves are a useful tool for identifying magnetic coercivity spectra in a test piece. Hysteresis properties such as saturation remanence ($M_s$), saturation magnetization ($M_{rs}$), remanent coercive force ($H_{cr}$), and coercive force ($H_c$), were plotted on a day plot (Day et al. 1977; Dunlop 2002) as a proxy for the magnetic grain size of ferromagnetic particles (e.g., Okada et al. 2017). At Nihon University, progressive thermal demagnetization of the IRMs imparted on three orthogonal axes (3-axis IRM tests; Lowrie 1990)

was performed to identify the constituent magnetic minerals of the pumice fall deposits by determining the Curie/Néel temperature. After demagnetizing the sample in a peak alternating magnetic field of 0.1 T using an alternating field demagnetized with a 3-axis tumbler system (DEM-8601; Natsuhara Giken), the magnetic fields of 2 T, 0.4 T, and 0.12 T were subsequently imparted on three orthogonal axes using an impulse magnetizer (IM-10-30; ASC Scientific) for the 3-axis IRM test. A thermal demagnetizer (DEM-8602; Natsuhara Giken) was used to perform stepwise thermal demagnetization in 20–50 °C increments up to 580 °C. The remanent magnetization was measured on a spinner magnetometer (SMD-88; Natsuhara Giken) after each demagnetization step. Additionally, MS was measured at each step to monitor potential thermal alteration of the heated specimen.

### Mineralogical analyses

Mineralogical analyses of opaque minerals were conducted at Nihon University using a JEOL-8800R electron probe microanalyzer (EPMA) at an accelerating potential of 15 kV and a probe current of 12 nA. The ZAF matrix correction method was used.

## Results

### Magnetic property measurements

The MS values of the pumice samples ranged between 240 and $400 \times 10^{-8}$ $m^3$/kg for the lower units (2p and 8p), whereas the values for the upper units (16p, 19p, and 21p) ranged between 180 and $360 \times 10^{-8}$ $m^3$/kg (Fig. 1d). The distribution ranges of the MS values of the samples were lower in the upper units than in the lower units. Therefore, the average MS values gradually decrease toward the upper units (Fig. 1d).

According to the MS results, higher MS samples from the 2p and 8p, as well as the lower MS samples from the 21 pm and 21pu were used in the subsequent experiments described below. Regardless of MS differences, the dominant magnetic minerals were of low coercivity, as evidenced by the IRM curves, which increase steeply at low fields and reach over 90% of the saturation magnetization by 0.2 T (Fig. 2a). Furthermore, the IRM acquisition curves are well fitted by a single magnetic component of a Burr type XII distribution (Zhao et al. 2018), indicating that the constituent magnetic minerals are the same across samples regardless of MS difference.

In the 3-axis IRM tests for the samples with both higher and lower MS values, the IRMs imparted with a magnetizing field of 0.12 T (indicated as "soft" in Fig. 2b) gently decreases upon heating, with a slightly sharp decrease in the medium components around 300 °C. This soft component is demagnetized up to 500 °C and completely erased by 580 °C (Fig. 2b), indicating that the remanent magnetization is predominantly carried by (titano)magnetite in the samples. However, the magnetization at 2 T was almost completely replaced by those imparted at 0.4 and 0.12 T, as evidenced by the negligible hard components in Fig. 2b, indicating the absence of high-coercivity minerals such as hematite. In addition, no significant changes in MS, an indicator of thermal alteration during stepwise thermal demagnetization in the 3-axis IRM test, were observed during the experiments (Fig. 2b). Generally, the hysteresis parameters of all samples fall in the pseudo-single domain (PSD) and multidomain (MD) regions on the Day plot (Fig. 2c), suggesting that the TM of large size grains is probably the dominant magnetic phase of the samples.

### Mineralogical analyses

The microscopic observations and mineralogical analyses indicated that regardless of MS magnitude, the opaque minerals included in the pumice fall deposits are TM, titanohematite (TH), and pyrrhotite (Po). The following are the two types of TM found in the deposits: (type I) a euhedral to subhedral crystal with no ilmenite lamellae indicating oxidation as shown in Haggerty (1991), occurring as isolated crystals or components of crystal clots with pyroxenes (Fig. 3a, b); (type II) a TM-orthopyroxene symplectite, which is rarely found in the study pumice regardless of MS magnitude and is derived from the breakdown of olivine because of magma mixing (e.g., Morgavi et al. 2016) or redox state change (e.g., Haggerty and Baker 1967) (Fig. 3c). The TM grains observed microscopically range from a few micrometers to tens of micrometers in diameter, indicating magnetic PSD to MD regions (e.g., Moskowitz 1980). The TH is an isolated euhedral crystal or bleb-shaped crystal associated with TM (Fig. 3b). The Po has a globular shape (Fig. 3d). Syn-eruptive breakdown of Po, shown by Matsumoto (2019) for the pumice fall deposit, is not found in the study specimens.

The average ulvöspinel content ($X_{usp}$, $0 \leq X_{usp} \leq 1$) of TM of type I of the higher MS sample from 2p is 0.35 (number of analyses: 46, $2\sigma$: 0.7 mol%), and that of the lower MS sample from 21pu is 0.35 (number of analyses: 61, $2\sigma$: 0.4) (Table 1 and Fig. 3e). The average $X_{usp}$ for type II, which has a distinct chemical composition, is 0.25 (number of analyses: 19, $2\sigma$: 0.05). Both types of TMs show no chemical zoning (Fig. 3f). The ilmenite content ($X_{il}$, $0 \leq X_{il} \leq 1$) of TH for both samples is around 0.78, indicating paramagnetism (Table 1, and Fig. 3e). The Po in the deposits contains a few weight percentages of impurities such as copper (Table 2). The mole fraction of FeS ($X_{FeS}$, $0 \leq X_{FeS} \leq 1$) in the $Fe_{S-S2}$ system ranges from 0.88 to 0.92.

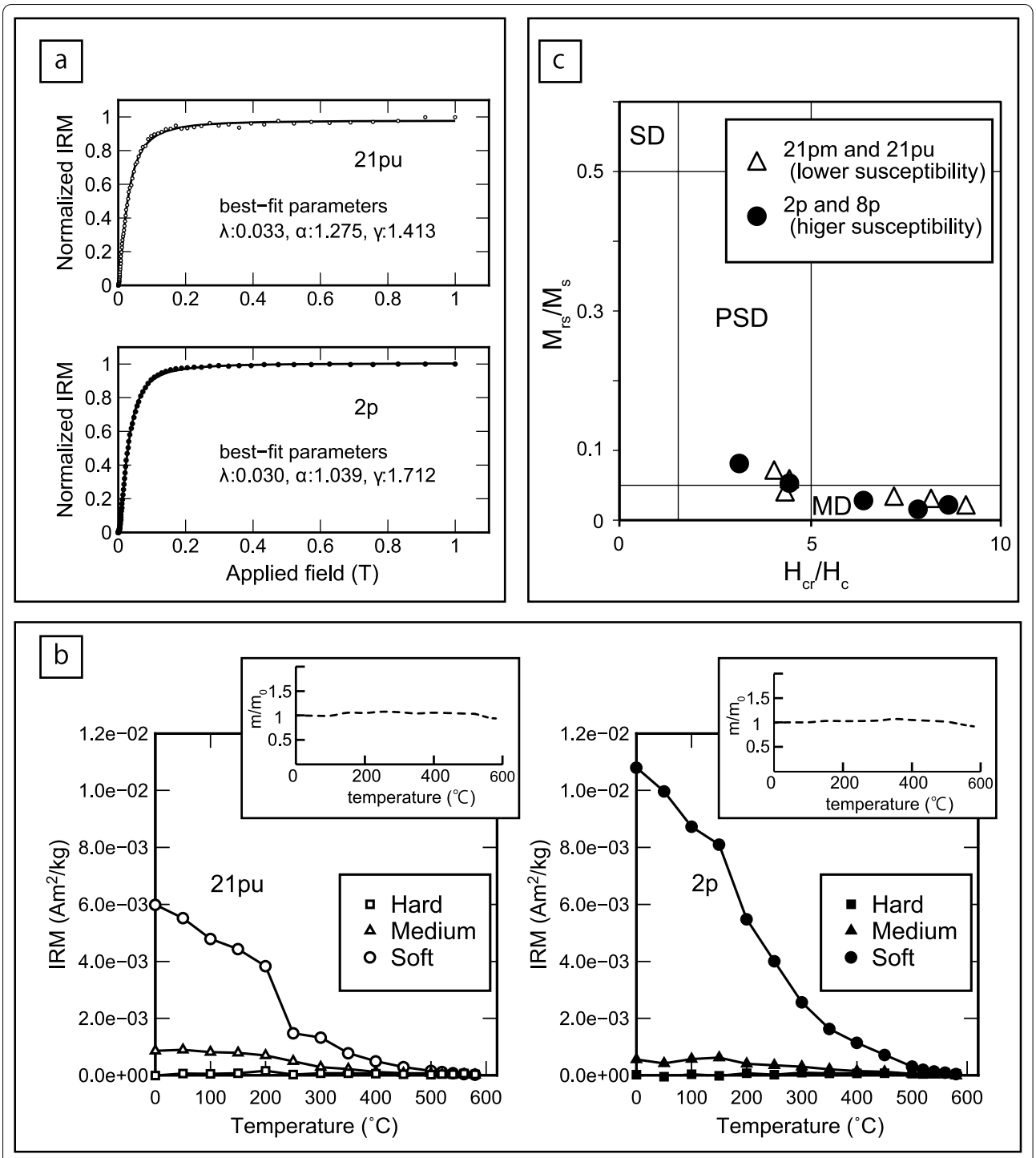


**Fig. 2** Rock magnetic experiments of the pumice fall deposits. **a** Diagrams showing IRM acquisition curves for two characteristic samples from 2 and 21pu. Both curves can be closely fitted by a single component of a Burr type XII distribution (solid lines) following the protocol of Zhao et al. (2018). The best-fitting parameters are listed in the diagrams. **b** Results of the 3-axis IRM tests for units 2p and 21pu. The insets on the upper right show the change in MS during stepwise thermal demagnetization. The vertical axis of the inset represents the rate of change of MS. $m_0$: unheated MS, $m$: MS in each step (**c**) Day plot for the pumice fall deposits (Day et al. 1977). $M_{rs}$: saturation remanence, $M_s$: saturation magnetization, $H_{cr}$: remanent coercive force, $H_c$: coercive force, SD: single domain, PSD: pseudo-single domain, MD: multidomain

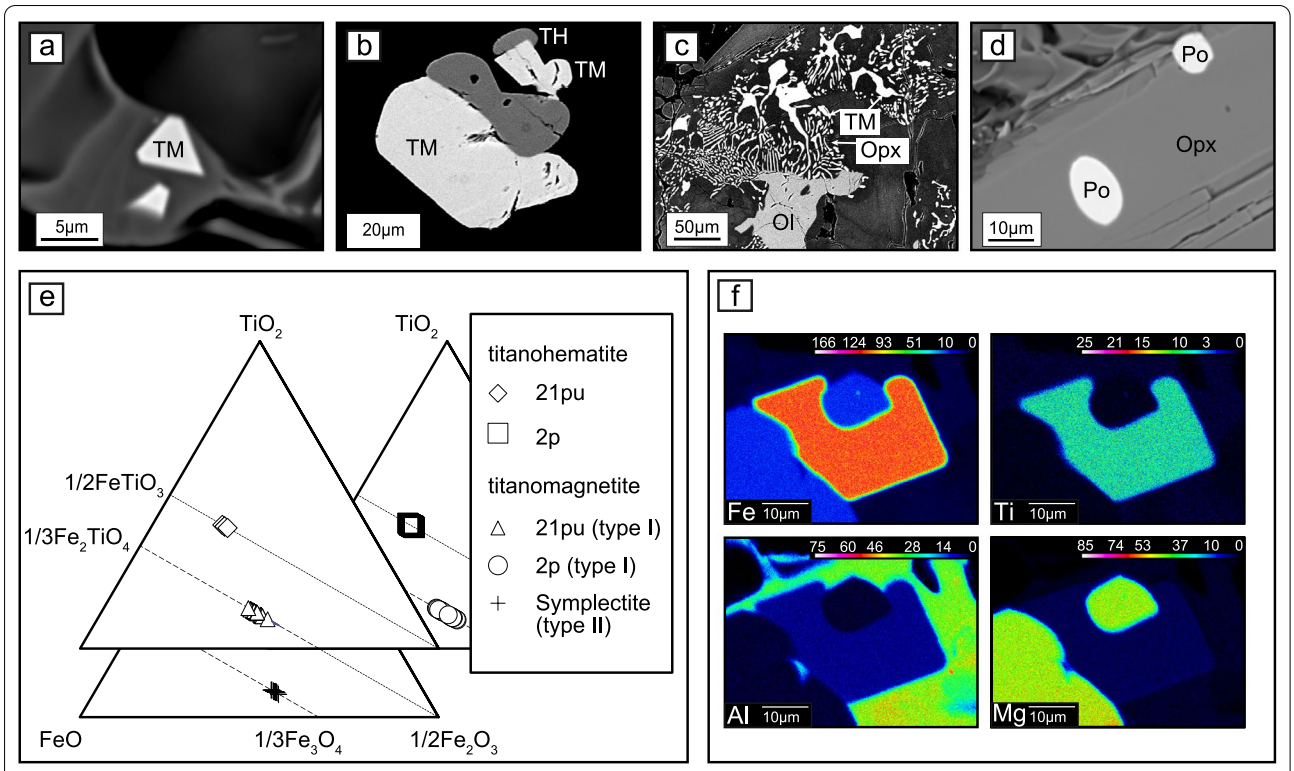


**Fig. 3** Representative back-scattered electron images (**a**–**d**) and electron probe analyses (**e**, **f**) of opaque minerals in the pumice fall deposits. **a** Euhedral homogeneous TM (type I) in volcanic glass. **b** Bleb-shaped TH associated with TM (type I). **c** TM–Opx symplectite (type II). **d** Globular pyrrhotite is included in orthopyroxene. *TM* titanomagnetite, *TH* titanohematite, *Opx* orthopyroxene, *Ol* olivine, *Po* pyrrhotite. **e** FeO-1/2$Fe_2O_3$–$TiO_2$ ternary diagrams showing chemical compositions of Fe–Ti oxides. The dashed and dotted lines indicate solid solutions of TM and TH, respectively. **f** Representative elemental maps of TM (type I) for Fe, Ti, Al, and Mg. The color bar beside each map indicates the relative intensity

**Table 1** Representative chemical compositions of Fe–Ti oxides

| No. | 1 | 2 | 3 | 4 | 5 | 6 | 7 |
|---|---|---|---|---|---|---|---|
| (wt.%) | | | | | | | |
| $SiO_2$ | 0.31 | 0.44 | 0.30 | 0.43 | 0.43 | 0.00 | 0.00 |
| $TiO_2$ | 9.49 | 13.41 | 13.51 | 11.21 | 8.77 | 42.41 | 42.11 |
| FeO* | 78.81 | 76.27 | 76.81 | 78.22 | 78.29 | 52.85 | 52.52 |
| MgO | 2.68 | 2.52 | 2.36 | 2.65 | 3.60 | 2.83 | 3.02 |
| $Al_2O_3$ | 3.17 | 2.55 | 2.53 | 2.68 | 3.47 | 0.36 | 0.34 |
| CaO | 0.54 | 0.06 | 0.00 | 0.00 | 0.02 | 0.04 | 0.03 |
| MnO | 0.31 | 0.36 | 0.33 | 0.35 | 0.27 | 0.28 | 0.27 |
| Total | 95.31 | 95.60 | 95.83 | 95.54 | 94.84 | 98.75 | 98.30 |
| Recalculated | | | | | | | |
| FeO | 35.76 | 40.11 | 40.44 | 38.06 | 34.44 | 32.77 | 32.18 |
| $Fe_2O_3$ | 47.84 | 40.19 | 40.42 | 44.63 | 48.73 | 22.31 | 22.61 |
| Total | 100.10 | 99.62 | 99.88 | 100.01 | 99.72 | 100.99 | 100.56 |
| $X_{usp}$ (mol%) | 27.26 | 38.77 | 36.41 | 32.54 | 25.63 | | |
| $X_{il}$ (mol%) | | | | | | 78.76 | 78.44 |

Nos. 1 and 2 are TM (Type I) of 2p. Nos. 3 and 4 are TM of 21pu. No. 5 is the TM (Type II) of symplectite. No. 6 is TH of 2p. No. 7 is TH of 21pu. FeO*: total iron as FeO. Recalculations for ferric iron contents are based on Carmichael (1967). $X_{usp}$ and $X_{il}$ are ulvöspinel content of TM and ilmenite content of TH, respectively

**Table 2** Representative chemical compositions of pyrrhotite

| | 2p | | 21pu | |
|---|---|---|---|---|
| | 1 | 2 | 3 | 4 |
| wt.% | | | | |
| Fe | 59.93 | 58.66 | 59.77 | 59.14 |
| Cu | 1.11 | 1.89 | 1.85 | 1.55 |
| S | 37.65 | 38.17 | 37.45 | 37.22 |
| Total | 98.69 | 98.72 | 99.06 | 97.91 |
| at.% | | | | |
| Fe | 47.38 | 46.26 | 47.20 | 47.18 |
| Cu | 0.77 | 1.31 | 1.29 | 1.09 |
| S | 51.85 | 52.43 | 51.52 | 51.73 |
| Total | 100 | 100 | 100 | 100 |

## Discussion

Regardless of the MS difference, the microscopic observations and mineralogical experiments agree well with the results of the magnetic experiments. The microscopic observations of TM grain size are consistent with the hysteresis properties of the samples, indicating that they are PSD to MD (Figs. 2c, 3a, b). The low coercivity spectra demonstrated by the IRM acquisition curves (Fig. 2a) and maximum unblocking (or Curie) temperature of less than 580 °C demonstrated by the 3-axis IRM tests (Fig. 2b) indicate that TM is the dominant remanent magnetization carrier. The gentle decreases in soft components in 3-axis IRM tests are common in rocks containing MD grains (e.g., Dunlop and Özdemir 1997, 2000; Yu and Dunlop 2006). Additionally, neither high-coercivity minerals such as hematite nor oxidation upon heating were detected in the 3-axis IRM tests, which is consistent with the microscopic observations and mineral chemistry. The unblocking temperature of the soft component in the 3-axis IRM tests implies that the chemical composition of TM, as the dominant magnetic carrier in the higher and lower MS samples, shows common characteristics (Fig. 2b). This is consistent with mineralogical analyses that show common $X_{usp}$ (Fig. 3e). Although the sharp decrease in the medium components around 300 °C in the 3-axis IRM tests may indicate the existence of Po, the IRM of this component has a negligible amplitude.

We take a closer look at the MS variation. Because the MS value of Po is at least two orders of magnitude lower than that of TM (Tarling and Hrouda 1993), it is assumed to have a negligible contribution to the bulk MS. Thus, in this study, we confine our attention to the TM as the MS carrier. Generally, the magnitude of the MS of a material varies based on mineralogy (such as type of mineral and its chemical composition), grain size, or abundance of magnetic minerals in the material. In terms of mineralogy, the results of our experiments indicate that TM is the dominant magnetic carrier in the samples regardless of the MS magnitude. Similarly, the grain size of the magnetic minerals, as determined by hysteresis analyses, does not differ between the higher and lower MS samples (Fig. 2c). Therefore, the MS variety of samples should be derived from the abundance of TM. Here, Yasui and Koyaguchi (2004) revealed that binary magma mixing dominated to form the eruption's ejecta and that one endmember magma, whose phenocrysts forming crystal clots tended to be surrounded by brownish glass, was relatively mafic but TM free, whereas the other endmember, whose phenocrysts tended to be surrounded by clear glass, was relatively felsic but contained TM. Yasui (2016) added that mineral assemblages of the two endmember magmas are the same as that of the crystal clots judging from the mineralogical study by Miura et al. (2007). Moreover, regardless of the MS magnitude, mineral chemistries of opaque minerals are not diverse indicating that the magmatic conditions, such as oxygen fugacity or temperature or both, did not change during the eruption. These imply that the modal percentage of TM in the mafic endmember was lower than that in the felsic endmember. Therefore, the difference in mixing ratio between the two endmember magmas must have caused the MS difference for the pumice fall deposits. The relationship between the MS value and contribution of the mafic endmember magma is shown in Fig. 1d, e. That is, the MS values become lower with the contribution of the mafic component in the histograms toward the upper unit of the succession (Fig. 1d, e). Herein, we successfully showed the relationship between magnetic petrology and the magmatic processes.

## Summary

The pumice fall deposits of the 1783 eruption of the Asama volcano were studied using magnetic petrology. We found that the MS of the deposits decreased gradually between the deposits of the preclimactic phase and that of the climactic phase, although other magnetic properties assumed by the magnetic property measurements (IRM acquisition curve, hysteresis analyses, and 3-axis IRM tests) show similar characteristics regardless of the magnitude of the MS. The variation of the MS for the deposits is our key finding, indicating a whole-rock chemical transition from felsic to mafic through magma mixing. However, the magnetic properties of the deposits agree with the mineralogical investigation, indicating that TM is the major magnetic component and Po has a minor contribution. However, we successfully showed that the magnetic petrological study accurately described the petrological features derived from the magmatic process. As previously stated, a careful magnetic petrological study can be a useful tool for detecting

the transition of magmatic and/or eruptive processes during a consecutive eruption. Rock magnetic measurements are superior to and faster than petrological experiments in bulk sample observations. It is a useful tool to quickly detect the state change of volcanic ejecta quickly. Magnetic susceptibility measurement, particularly, can be measured easily in the field and has potential for wide use. For example, successive MS observations for pyroclastic ejecta, such as ash from a frequent Vulcanian eruption of an active volcano, must be worth measuring.

#### Abbreviations

AGM: Alternating gradient magnetometer; AVO: Asama Volcano Observatory; EPMA: Electron probe microanalyzer; MS: Mass-specific magnetic susceptibility; IRM: Isothermal remanent magnetization; NIPR: National Institute of Polar Research; T: Tesla; TH: Titanohematite; TM: Titanomagnetite; XRF: X-ray fluorescence.

#### Acknowledgements

We thank Prof. Maya Yasui (Nihon Univ.) for allowing to use a part of the figure from her study. We are also grateful to two anonymous reviewers for helpful comments. The topographic map in Fig. 1a was made by the author (TK) using the Fundamental Geospatial Data 10 m DEM, which was published by the Geospatial Information Authority of Japan. The authors would like to thank Enago (www.enago.jp) for their English language review.

#### Author contributions

TK contributed to the fieldwork and the whole-rock chemistry, mineralogical, and magnetic property measurements. KF contributed to the fieldwork. YS and XZ contributed to the magnetic property measurements. All authors contributed to the discussion and writing of the manuscript. All authors read and approved the final manuscript.

#### Funding

No funding was received.

#### Availability of data and materials

The experimental data referred to in the paper are available from the corresponding author on reasonable request.

## Declarations

#### Ethics approval and consent to participate

Not applicable.

#### Competing interests

The authors declare that they have no competing interests.

#### Author details

[1]Department of Earth and Environmental Sciences, College of Humanities and Sciences, Nihon University, 3-25-40, Sakurajosui, Setagaya-ku, Tokyo 156-8550, Japan. [2]Faculty of Business Administration, Aichi University, 4-60-6 Hiraike-cho, Nakamura-ku, Nagoya-shi, Aichi 453-8777, Japan. [3]National Institute of Polar Research, 10-3 Midoricho, Tachikawa, Tokyo 190-8518, Japan. [4]School of Oceanography, Shanghai Jiao Tong University, 1954 Huashan Rd., Shanghai 200030, China. [5]Department of Polar Science, School of Multidisciplinary Sciences, The Graduate University for Advanced Studies (SOKENDAI), 10-3 Midoricho, Tachikawa, Tokyo 190-8518, Japan.

Received: 23 December 2021 Accepted: 31 March 2022
Published online: 13 April 2022

#### References

Aramaki S (1956) The 1783 activity of Asama volcano, part 1. Jpn J Geol Geogr 27:189–229

Aramaki S (1957) The 1783 activity of Asama volcano, part 2. Jpn J Geol Geogr 28:11–33

Aramaki S (1963) Geology of Asama volcano. J Fac Sci Univ Tokyo 14(2):29–443

Aramaki S, Takahashi M (1992) Geology and petrology. In: Guide book for field workshop at Asama and Kusatsu-Shirane volcanoes, Japan. IAVCEI Commission on Explosive Volcanism

Aramaki S (1993) Geological map of Asama volcano. Geological survey of Japan 1:50,000 geologic map and explanatory text (**in Japanese with English summary**)

Carmichael ISE (1967) The iron-titanium oxides of salic volcanic rocks and their associated ferromagnesian silicates. Contrib Mineral Petrol 14:36–64

Day R, Fuller M, Schmidt VA (1977) Hysteresis properties of titanomagnetites: grain size and compositional dependence. Phys Earth Planet Inter 13:260–267. https://doi.org/10.1016/0031-9201(77)90108-X

Dunlop DJ (2002) Theory and application of the Day plot (Mrs/Ms versus Hcr/Hc) 1. Theoretical curves and tests using titanomagnetite data. J Geophys Res Solid Earth 107:EPM4-1-EPM4-22. https://doi.org/10.1029/2001JB000486

Dunlop DJ, Özdemir Ö (1997) Rock magnetism: fundamentals and frontiers. Cambridge University Press, Cambridge

Dunlop DJ, Özdemir Ö (2000) Effects of grain size and domain state on thermal demagnetization tails. Geophys Res Lett 27:1311–1314. https://doi.org/10.1029/1999GL008461

Frost BR (1991) Magnetic petrology: factors that control the occurrence of magnetite in crustal rocks. In: Lindsley DH (ed) Oxide minerals: petrologic and magnetic significance, reviews in mineralogy, vol 25. Mineralogical Society of America, Chelsea, pp 489–509

Haggerty SE (1991) Oxide textures—a mini-atlas. In: Lindsley DH (ed) Oxide minerals: petrologic and magnetic significance, reviews in mineralogy, vol 25. Mineralogical Society of America, Chelsea, pp 129–219

Haggerty SE, Baker I (1967) The alteration of olivine in basaltic and associated lavas Part I: high temperature alteration. Contrib Mineral Petrol 16:233–257. https://doi.org/10.1007/BF00371095

Imai H, Mikada H (1982) The 1783 activity of Asama volcano inferred from the measurements of bulk density of tephra (pumice) and the old documents. Bull Volcanol Soc Japan 27:27–43 (**in Japanese with English abstract**)

Lowrie W (1990) Identification of ferromagnetic minerals in a rock by coercivity and unblocking temperature properties. Geophys Res Lett 17:159–162. https://doi.org/10.1029/GL017i002p00159

Matsumoto K (2019) Pyrrhotite oxidation as a proxy for thermal structure of eruption clouds: a comparative study of Plinian and vulcanian eruptions of Asama and Sakurajima volcanoes, Japan. J Volcanol Geotherm Res 392:106758. https://doi.org/10.1016/j.jvolgeores.2019.106758

Miura K, Takahashi M, Yasui M (2007) Comparative petrography for plagioclase phenocryst in volcanic rocks of historical large-scale eruptions of Asama–Maekake volcano, Central Japan. Proc Inst Nat Sci Nihon Univ 42:117–128 (**in Japanese with English abstract**)

Morgavi D, Arzilli F, Pritchard C, Perugini D, Mancini L, Larson P, Dingwell DB (2016) The Grizzly Lake complex (Yellowstone Volcano, USA): mixing between basalt and rhyolite unraveled by microanalysis and X-ray microtomography. Lithos 260:457–474. https://doi.org/10.1016/j.lithos.2016.03.026

Moskowitz BM (1980) Theoretical grain size limits for single-domain, pseudo-single-domain and multi-domain behavior in titanomagnetite (x = 0.6) as a function of low-temperature oxidation. Earth Planet Sci Lett 47:285–293. https://doi.org/10.1016/0012-821X(80)90045-X

Nagata T (2013) Identification of magnetic minerals in rocks using methods based on their magnetic properties. In: Collinson DW, Creer KM, Runcorn SK (eds) Methods in palaeomagnetism, vol 3. Developments in solid earth geophysics. Elsevier, Amsterdam, pp 501–513. https://doi.org/10.1016/B978-1-4832-2894-5.50086-0

Nakamura M (1995) Continuous mixing of crystal mush and replenished magma in the ongoing Unzen eruption. Geology 23:807–810. https://doi.org/10.1130/0091-7613(1995)023%3c3C0807:CMOCMA%3e3E2.3.CO;2

Okada M, Suganuma Y, Haneda Y, Kazaoka O (2017) Paleomagnetic direction and paleointensity variations during the Matuyama-Brunhes polarity transition from a marine succession in the Chiba composite section of

the Boso Peninsula, central Japan. Earth Planet Space 69:45. https://doi.org/10.1186/s40623-017-0627-1
Saito T, Ishikawa N, Kamata H (2007) Magnetic petrology of the 1991–1995 dacite lava of Unzen volcano, Japan: degree of oxidation and implications for the growth of lava dome. J Volcanol Geotherm Res 164:268–283. https://doi.org/10.1016/j.jvolgeores.2007.05.015
Takahashi M, Mukai Y, Nakajima T, Yasui M, Kanamaru T (2008) Wole-rock major element chemistry for eruptive products of Asama–Hotokeiwa volcano: summary for data of 307 samples. Proc Inst Nat Sci Nihon Univ 43:167–193 (**in Japanese with English abstract**)
Takahashi M, Ichikawa H, Kanamaru T, Yasui M, Maseguchi M (2013) Proximal Volcaniclastic rocks of the Asama–Kurofu volcano at the Sennin-iwa located in the wall of Kurofu sector-collapsed caldera: volcanic breccias and tuff breccias of the Gippa Lava group and welded pyroclastic rocks of the Sennin lava group. Proc Inst Nat Sci Nihon Univ 48:141–168 (**in Japanese with English abstract**)
Tamura C, Hayakawa Y (1995) Reconstruction of the sequence of the 1783 Asama eruption from the ancient literature. J Geogr 104:843–864 (**in Japanese with English abstract**)
Tarling DH, Hrouda F (1993) The magnetic anisotropy of rocks. Chapman & Hall, London, p 217p
Tsukui M (2010) The 1783 eruption of Asama volcano: ash-fall distribution and sequence of the eruption review from old documents. Bull Volcanol Soc Japan 56:65–87 (**in Japanese with English abstract**)
Turner MB, Cronin SJ, Stewart RB, Bebbington M, Smith IEM (2008) Using titanomagnetite textures to elucidate volcanic eruption histories. Geology 36:31–34. https://doi.org/10.1130/G24186A.1
Yasui M (2016) Petrography of the Asama 1783 eruptive products. Proc Inst Nat Sci Nihon Univ 51:231–255 (**in Japanese with English abstract**)
Yasui M, Koyaguchi T (2004) Sequence and eruptive style of the 1783 eruption of Asama volcano, central Japan: a case study of an andesitic explosive eruption generating fountain-fed lava flow, pumice fall, scoria flow and forming a cone. Bull Volcanol 66:243–262. https://doi.org/10.1007/s00445-003-0308-8
Yasui M, Koyaguchi T, Aramaki S (1997) Plinian eruption in the 1783 activity of Asama volcano inferred from the deposits and the old records. Bull Volcanol Soc Japan 42:281–297 (**in Japanese with English abstract**)
Yu Y, Dunlop D (2006) Testing the independence of partial thermoremanent magnetizations of single-domain and multidomain grains: implications for paleointensity determination. J Geophys Res 111:B12S31. https://doi.org/10.1029/2006JB004434
Zhao X, Fujii M, Suganuma Y, Zhao X, Jiang Z (2018) Applying the Burr Type XII distribution to decompose remanent magnetization curves. J Geophys Res Solid Earth 123(10):8298–8311. https://doi.org/10.1029/2018JB016082

## Publisher's Note